Validation of middle-atmosphere carbon monoxide retrievals from the Microwave Limb Sounder on Aura

H. C. Pumphrey, M. J. Filipiak, N. J. Livesey, M. J. Schwartz, C. Boone, K. A. Walker, P. Bernath, P. Ricaud, Brice Barret, Cathy Clerbaux, et al.

Validation of middle-atmosphere carbon monoxide retrievals from the Microwave Limb Sounder on Aura

H. C. Pumphrey,[1] M. J. Filipiak,[1] N. J. Livesey,[2] M. J. Schwartz,[2] C. Boone,[3] K. A. Walker,[3,4] P. Bernath,[3,5] P. Ricaud,[6] B. Barret,[6] C. Clerbaux,[7] R. F. Jarnot,[2] G. L. Manney,[2,8] and J. W. Waters[2]

Received 30 March 2007; revised 22 June 2007; accepted 24 July 2007; published 29 December 2007.

[1] The Microwave Limb Sounder on Aura has produced an extensive set of measurements of CO in the middle atmosphere. The measurements are usable for scientific studies from the upper troposphere up to 90 km altitude. We describe these measurements and validate them by demonstrating their internal consistency and by comparing them to other remotely sounded measurements and to 2-D model simulations. Comparisons with other measurements suggest that MLS has a positive bias of 25–50% in the mesosphere and a negative bias of up to 70% in the (almost CO-free) lower stratosphere. The geophysical features observed in the MLS CO field show excellent qualitative agreement with other measurements.

Citation: Pumphrey, H. C., et al. (2007), Validation of middle-atmosphere carbon monoxide retrievals from the Microwave Limb Sounder on Aura, *J. Geophys. Res.*, *112*, D24S38, doi:10.1029/2007JD008723.

1. Introduction

[2] Carbon monoxide (CO) in the atmosphere has three main sources: combustion at the Earth's surface, oxidation of methane in the stratosphere, and the photolysis of carbon dioxide in the mesosphere and thermosphere [*Solomon et al.*, 1985; *Allen et al.*, 1999]. The main loss mechanism is oxidation by the OH radical. The balance between the sources and the sink leads to relatively large mixing ratios of CO in the troposphere and the upper mesosphere, with extremely small mixing ratios in the lower stratosphere. The lifetime of CO varies from 5–10 d in the upper stratosphere to over 40 d at the mesopause and in the lower stratosphere [*Allen et al.*, 1999], so that the diurnal cycle is small and the molecule acts as a tracer of atmospheric motion. The first measurement of CO in the mesosphere was made using a microwave technique [*Waters et al.*, 1976] and was consistent with the general picture that we have described.

[3] The Microwave Limb Sounder [*Waters*, 2006] (MLS) on the Aura satellite has made daily global measurements of the mixing ratio of CO since August 2004. These are the most extensive set of measurements to date of middle-atmosphere CO. In this paper we describe the measurements, show that they are internally consistent, and compare them to several other data sets. We restrict ourselves to the stratosphere and mesosphere; clouds and spatial variability mean that the upper troposphere presents a sufficiently different problem of both validation and measurement that it is considered in a separate paper [*Livesey et al.*, 2007]. We describe the second publicly released version of the MLS data: version 2.2. For CO, this is a substantial improvement on the previous release (version 1.5); we briefly describe the differences between the two versions.

2. MLS Measurements

2.1. Overview

2.1.1. Instrument

[4] The MLS instrument [*Waters*, 2006] is essentially a small radio telescope. It flies on the Aura satellite [*Schoeberl et al.*, 2006] which is in a Sun-synchronous near-circular polar orbit; the nominal south-to-north equator-crossing time is 1345 UT. MLS views the limb looking forward from the satellite, so that the latitudinal coverage is from 82°S to 82°N every day. The antenna scans the limb exactly 240 times per orbit and there are approximately 14.5 orbits per day. Each scan across the limb provides radiance measurements at 120 tangent altitudes. These are spaced 300 m apart in the troposphere, 1.5 km apart in the stratosphere and lower mesosphere and 3 km apart in the upper mesosphere. The radiation received from the atmosphere is fed from the antenna to five heterodyne radiometers covering spectral regions near 118 GHz (two polarizations), 191 GHz, 240 GHz and 640 GHz. (A sixth radiometer at 2500 GHz is fed by a separate antenna.) The output of the five GHz radiometers is analyzed by 26

[1]School of Geosciences, University of Edinburgh, Edinburgh, UK.
[2]NASA Jet Propulsion Laboratory, Pasadena, California, USA.
[3]Department of Chemistry, University of Waterloo, Waterloo, Ontario, Canada.
[4]Also at Department of Physics, University of Toronto, Toronto, Ontario, Canada.
[5]Also at Department of Chemistry, University of York, York, UK.
[6]Laboratoire d'Aerologie, Toulouse, France.
[7]Service d'Aeronomie/Institut Pierre-Simon Laplace, Centre National de la Recherche Scientifique, Université Pierre et Marie Curie-Paris 6, Paris, France.
[8]Also at New Mexico Institute of Mining and Technology, Soccoro, New Mexico, USA.

0148-0227/07/2007JD008723

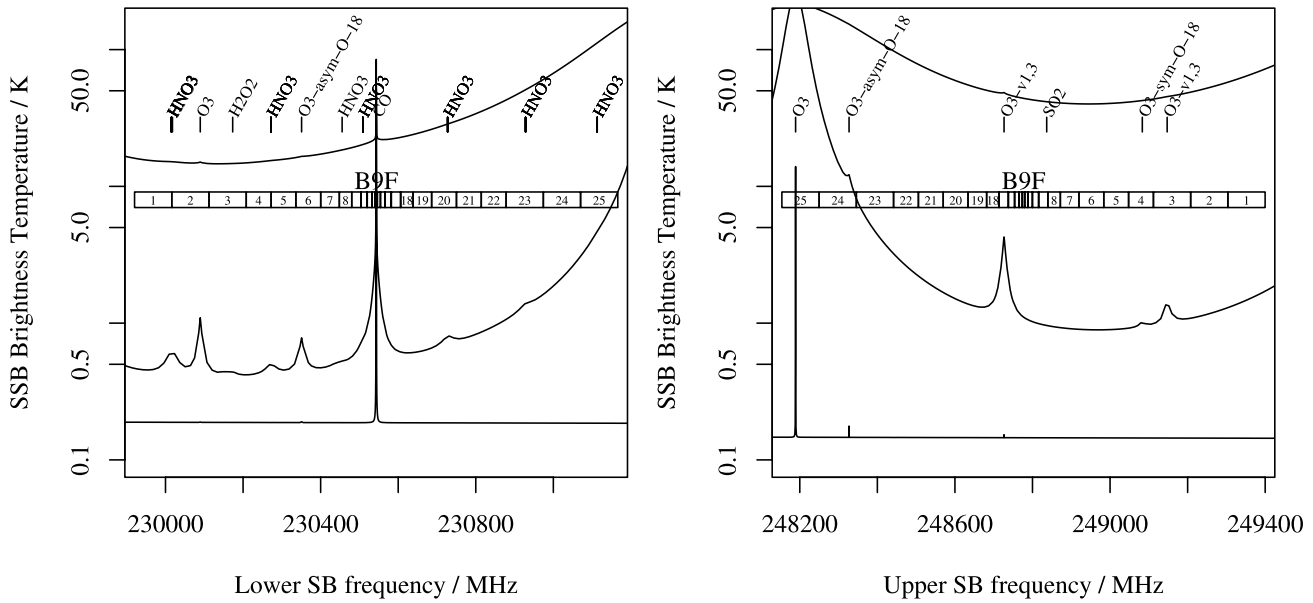

Figure 1. Calculated radiance spectra for the two parts of the spectrum detected by band 9 of MLS. The numbered boxes indicate the 25 channels which make up the band. The DACS (band 25) covers approximately the same spectral region as the center channel of band 9. The measured radiance is the sum of the values from the (left) lower sideband and (right) upper sideband. The three curves are for tangent altitudes of 20 km (top), 35 km and 80 km (bottom). The positions of various spectral lines are marked: the main interfering species are O_3 and HNO_3, including various isotopic and vibrationally excited variants. The target CO line is in the center of the lower sideband.

spectrometers: 22 filter banks and 4 digital autocorrelator spectrometers (DACS). Most of the filter banks are located so that they cover a frequency range centered on a single spectral line of a target molecule. Microwave spectral lines show strong pressure broadening: a line which is 1 MHz wide at 0.3 hPa (56 km) will be 300 MHz wide at 100 hPa (16 km). For this reason the filter banks are implemented with narrower filters toward the band center. The heterodyne nature of the radiometers means that each spectrometer is affected by two quite separate spectral regions or sidebands, one on each side of the local oscillator (LO) frequency. The sideband not containing the target line is not filtered out. Instead, the LO frequency is chosen so that, for the most important measurements, the nontarget sideband is in a spectral region with no strong lines. (The 118 GHz radiometer is an exception; it is a single-sideband radiometer.)

[5] The MLS carbon monoxide measurements are made by the 240 GHz radiometer. This has one filter bank (band 9, abbreviated to B9F) and one DACS (band 25, abbreviated to B25D) centered on the 230.538 GHz spectral line of CO. Band 9 consists of 25 channels with widths ranging from 6 MHz to 96 MHz, giving a total width of over 1 GHz. Band 25 consists of 129 channels with a width of 97.6 kHz giving a total width of 12.5 MHz. Figure 1 shows radiances arriving at the MLS radiometer in each sideband, calculated with a radiative transfer model. Note how the lines broaden rapidly as the altitude decreases. This is another factor which makes retrievals in the upper troposphere a different, and more difficult, problem.

2.1.2. Retrieval Technique

[6] The MLS retrieval technique is described in detail by *Livesey et al.* [2006]. Very briefly, the optimal estimation formula [*Rodgers*, 2000] is used, with one profile being retrieved for each scan. As the instrument view is along the direction of travel and retrieved profiles are spaced by only 1.5° great circle arc, the atmospheric region covered by several retrieved profiles influences the radiances measured from an individual scan. To handle this tomographic aspect of the measurement, the state vector **x** is a "chunk" of about 12 profiles and the measurement vector **y** is 12 scans. The chunks overlap slightly; the final product is constructed by discarding the end profiles from each chunk. The forward model is sufficiently nonlinear that a Marquardt-Levenberg technique is required to find the solution.

2.2. Radiance Spectra and Residuals

[7] For the retrieval to be internally consistent, we require that radiances calculated from the retrieved profile are in agreement with the original measurements. By "in agreement" we mean that the differences are of a similar size to the measurement noise. In Figure 2 we show zonal mean radiances and residuals, that is, the difference between measured and calculated radiances, for band 9. Approximately 200 spectra were averaged together to make Figure 2. All spectra came from a single day, from a latitude bin centered at 80°N. Other days and other latitude bins are similar. The dashed lines show the expected level of random noise in the averaged data; the noise on a single scan is $\sqrt{200} \approx 14$ times larger than this. Clearly the retrieval is achieving closure to within the single-profile measurement

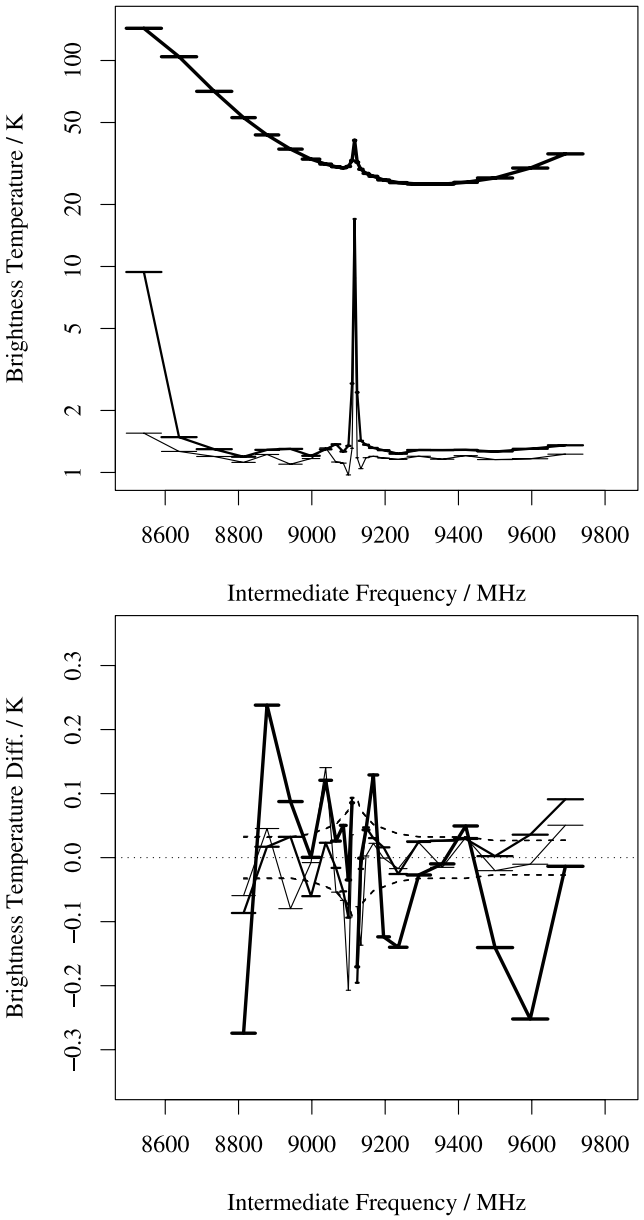

Figure 2. (top) Radiances and (bottom) residuals (measured radiances – calculated radiances) for band 9. All quantities are mean daily values for a 10° latitude bin centered at 80°N. The lines are for tangent heights of 20 km (thick), 45 km and 70 km (thin). Note that residuals are shown only for channels that are used in the retrieval. Channels 23–25 (at the left-hand side of the figure) are not used owing to the strong signal from ozone. The dashed lines are the expected 1-σ random error in this average, that is, the random error on a single measurement divided by square root of the number of profiles in the latitude bin. The target CO line appears at an intermediate frequency of 9117 MHz.

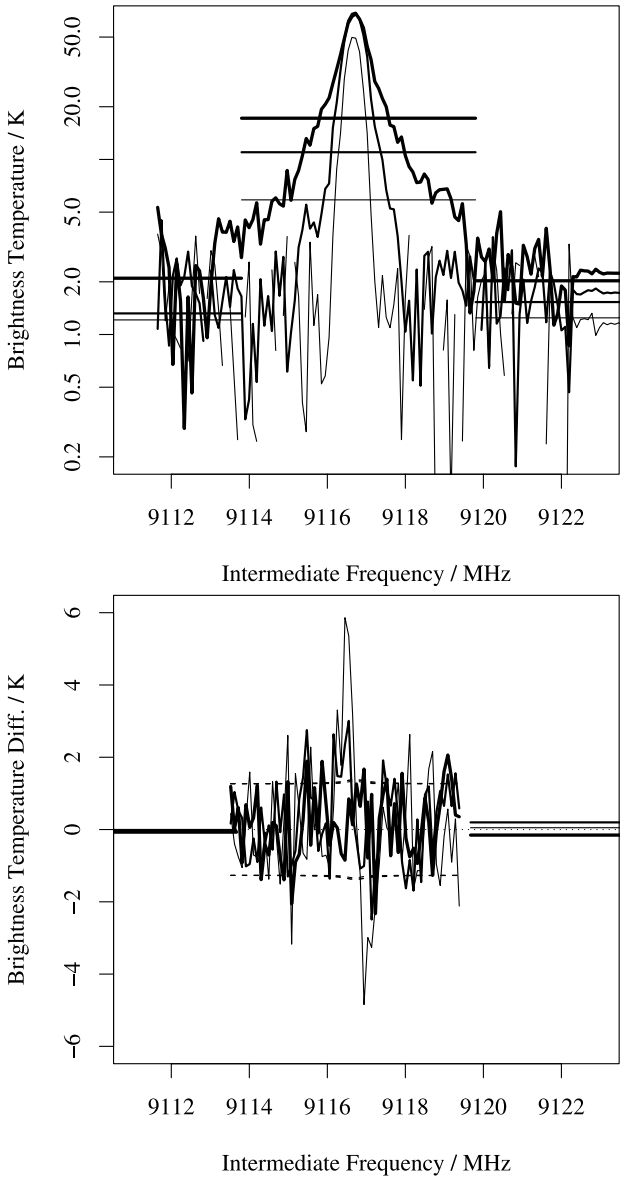

Figure 3. (top) Radiances and (bottom) residuals (measured radiances – calculated radiances) for DACS band 25. All quantities are mean daily values for a 10° latitude bin centered at 80°N. The lines are for tangent heights of 50 km (thick), 65 km and 80 km (thin). Channels 12–14 of band 9 are also visible in the plot. Note that residuals are shown only for channels that are used in the retrieval: Channel 13 of band 9 is not used as the DACS makes the information it would provide entirely redundant. DACS channels are not used where they overlap band 9 channels 12 and 14. The dashed lines are the expected 1-σ random error in this average, that is, the random error on a single measurement divided by the square root of the number of profiles in the latitude bin. The residuals exceed this near the line center, where there is a noticeable Doppler shift caused by wind that is not modeled. The target CO line appears at an intermediate frequency of 9117 MHz.

noise. However, Figure 2 suggests that there are spectral features in the residuals at a level of 0.2 K. This in turn implies that there are aspects of the measurement or the spectroscopy which are only understood to an accuracy of

Table 1. Meaning of Bits in "Status"[a]

Bit	Value	Meaning
0	1	do not use this profile (see bits 8–9 for details)
1	2	profile questionable (see bits 4–6 for details)
2	4	unused
3	8	unused
4	16	may have been affected by high-altitude clouds
5	32	may have been affected by low-altitude cloud
6	64	GEOS-5 data not used for temperature a priori
7	128	unused
8	256	retrieval diverged or too few radiances available
9	512	task retrieving this chunk crashed

[a]Bits marked "unused" are reserved for use in future versions and should never be set in version 2.2 data.

0.2 K and which could cause significant systematic errors in an average of several hundred profiles. In Figure 3 we show radiances and residuals for band 25. Again, the residuals are much smaller than the noise on a single scan. However, near the line center, they are larger than the noise expected on the average shown. The difference is probably caused by an unmodeled Doppler shift; it is unlikely to cause a noticeable error in the retrieved mixing ratio.

2.3. Data Usage and Screening

[8] The data are provided in HDF-EOS5 format. In addition to the field containing the retrieved volume mixing ratio ("L2gpValue") the files contain several additional fields which indicate the quality of the retrieved profile. The field "L2gpPrecision" is the diagonal elements of the covariance matrix, $\hat{\mathbf{S}}$, of the retrieved state vector $\hat{\mathbf{x}}$. This field contains error contributions from the measurement error and the smoothing error. Where the magnitude of "L2gpPrecision" is greater than 50% of the a priori error, the sign of this field is set to be negative. Data should not be used if the corresponding element of "L2gpPrecision" is negative.

[9] The field "Status" is a single integer for each profile, which is to be regarded as a set of 32 binary flags. The meanings of these flags are the same for all MLS products and are indicated in Table 1. A profile should not be used if any of bits 0, 8 or 9 are set. For the middle atmosphere there is no need to reject CO profiles with bit 4 set. (Note that bit 5 is not used for CO, or any other products of the 240 GHz radiometer.) If set at all, bit 6 should be set for a whole day, to indicate that no meteorological assimilation was available as a priori values for temperature and that a climatological zonal mean was used instead. The CO data should be usable under these circumstances, but should be treated with caution. The field "Quality" gives an indication of whether the retrieved profile is consistent with the measured radiances. "Quality" is calculated as $1/\chi^2$, where

$$\chi^2 = (\mathbf{y} - F(\mathbf{x}))^T \mathbf{S}_y^{-1} (\mathbf{y} - F(\mathbf{x}))$$

[10] Here, F is the forward model and $\mathbf{S}_y$ is the covariance matrix of the measurement noise. Only those radiances which have a significant effect on the CO product are included in the measurement vector $\mathbf{y}$ for this calculation. On inspecting the version 2.2 data, no clear relationship is observed between obviously bad CO profiles in the middle atmosphere and "Quality," possibly because the calculation is dominated by the troposphere. For CO, "Quality" usually lies between 1.5 and 3; as a precaution it is suggested that profiles should be rejected if "Quality" is less than 0.2. The field "Convergence" is a ratio of χ^2 at the end of the retrieval process to the value predicted at the previous step. This ratio should be close to unity; profiles with "Convergence" > 1.8 are clearly wrong in most cases and should always be rejected.

[11] CO is the second commonest molecule in the interstellar medium (after H_2). Its rotational lines have been used by radio-astronomers to survey the distribution of gas clouds in the Milky Way [*Combes*, 1991]. The 115 GHz line is the most popular for this purpose, but the 230 GHz line has also been used [*Oka et al.*, 1996]. The strongest emissions at this frequency come from the relatively dense gas clouds near the core of the Galaxy. For two periods during the year, 26 May to 23 June and 11 November to 13 December, the MLS CO data are contaminated by the presence of the core of the Galaxy in the instrument's field of view (FoV). In both periods, the affected profiles lie in a 20°-wide band of latitudes on one side of the orbit only. The May period affects profiles within 10° of 60°N on the descending (night) side of the orbit, while the November period affects profiles within 10° of 60°S on the ascending side of the orbit. The contamination is much stronger in the first two weeks of each period.

[12] The MLS retrieval software rejects those radiances affected by the brightest part of the galactic core, but this does not entirely prevent the surrounding regions of the galaxy from affecting the CO profiles. Furthermore, although the software rejects all channels of band 9 when the core is in the FoV, it does not reject band 25 or the other bands in the 240 GHz radiometer. As a result, the affected profiles do not have bit 7 of "Status" set, nor is "L2gpPrecision" set negative. Users should therefore reject all profiles from the times and latitudes described above. In some cases, but not all, the presence of the galactic core causes "Quality" to be considerably larger than usual. Users should reject profiles for which "Quality" is greater than 3.5 as an additional precaution, but the only safe way to filter out the galactic core is by date and latitude.

2.4. Data Precision and Resolution

2.4.1. Resolution

[13] The averaging kernels for the retrieval of CO are shown in Figure 4. The full width at half maximum of the kernels is 3–4 km below 60 km and 7–8 km above 60 km. This is more or less the resolution of the retrieval grid, which has 6 levels per pressure decade below the 0.1 hPa level and 3 levels per pressure decade above this. The tomographic nature of the retrieval as described in section 2.1.2 means that we need to consider the horizontal resolution as well. The complete averaging kernels include both horizontal and vertical dimensions; the vertical averaging kernels shown in Figure 4 are formed by integrating the complete kernels in the horizontal dimension for 5 along-track scans. The profile positions are spaced approximately 165 km apart along the measurement track; inspection of the horizontal averaging kernels (not shown) indicates that the resolution along this direction is in the range 200–330 km. In the direction perpendicular to the measurement track, the mea-

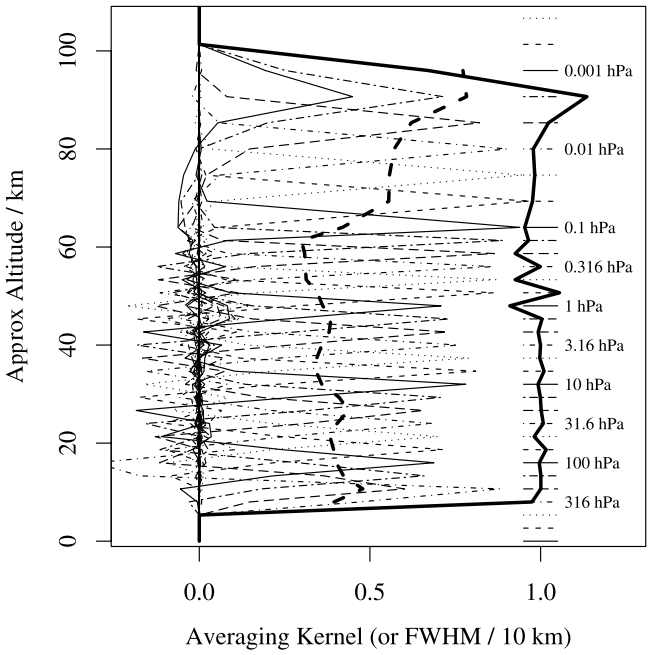

Figure 4. Averaging kernels for the retrieval of CO mixing ratio. The thick black line is the integrated kernel: values near unity indicate that almost all the information at that level was contributed by the measurement system, whereas lower values indicate increasing contributions from the a priori information. The thick dashed line is the full width at half-maximum of the averaging kernel. The "approximate altitude" vertical coordinate used here and in later figures is $16(3 - \log_{10}(\text{Pressure/hPa}))$. The kernels in this figure are for the equator, but those at other latitudes are very similar.

surement footprint is approximately 6 km across. The distance between measurements depends on latitude; away from the limiting latitudes of ±82°, adjacent orbits are about 24° of longitude apart.

2.4.2. Precision and Noise

[14] The precision values supplied with the data (field "L2gpPrecision" in the data files) are the diagonal elements of the covariance matrix of the retrieved profile, $\hat{\mathbf{S}}$; we shall refer to them as the retrieved precision. They contain contributions from the measurement noise and from smoothing error [see *Rodgers*, 2000]. This means that the random scatter in the data should be no larger than the retrieved precision. Where the a priori makes a large contribution to the retrieved profile, the random scatter should be much smaller than the retrieved precisions. We checked this by examining the scatter in the retrieved data within 10° of the equator, where there is expected to be little natural variability in the mixing ratio. Figure 5 shows that the standard deviation in the data is consistently smaller than the retrieved precision, by a factor of approximately 0.7. At low latitudes, the retrieved precision and scatter for single profiles are greater than 100% of the mixing ratio for altitudes between 20 and 70 km, so some averaging is needed to make use of the data. For example, a daily zonal mean with latitude bins of 10° will have a usable signal-to-noise ratio over all of the middle atmosphere. Near the winter pole the CO mixing ratios are larger than the precision over a much larger altitude range, because of descent of CO-rich air in the polar vortex.

[15] Both the high vertical resolution and high noise of the CO product are the result of choosing large a priori errors and only a small smoothing constraint. This was considered necessary for CO to reduce biases in the region of the vortex edge, where the mixing ratio can vary by orders of magnitude over a short distance. An appropriate a priori for regions outside the vortex would constrain the profile unacceptably inside it.

2.5. Estimate of Systematic Uncertainties

[16] The retrieved precisions ("L2gpPrecision") provided with the data do not include the vast majority of systematic error sources. (They do include the smoothing error, which is supposed to account for any errors in the a priori and which could in some ways be considered as a systematic error.) In this section we estimate the various systematic contributions to the total error in the retrieved CO mixing ratio. The errors are estimated by an end-to-end exercise of the retrieval system. Beginning with a set of profiles that we regard as "truth," we generate a set of simulated radiances using the forward model, and then retrieve a set of profiles to match the truth. This set of retrieved profiles are regarded as the base for comparisons. The set of profiles chosen consists of two orbits which sample the SLIMCAT chemical transport model (CTM) [*Chipperfield*, 1999]. The CTM was driven with meteorological data from 1996; the day chosen for the tests was 20 February. We next perturb the forward model in a number of ways, and feed the resulting radiances into the retrieval program. The results of each of these tests

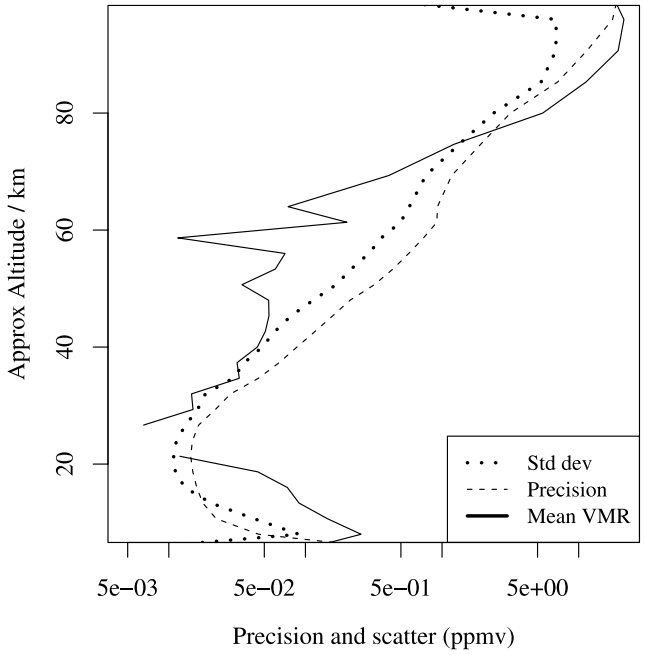

Figure 5. Retrieved precision and standard deviation of MLS version 2.2 CO data within 10° of latitude of the equator. The mean volume mixing ratio (VMR) is shown for comparison. Data are from 3 March 2006.

are compared to the base case. In addition, we compare the base case to the truth to estimate the errors due to numerical issues in the retrieval code. Each perturbation corresponds to either a 2-σ estimate of uncertainty in the relevant parameter or an estimate of the maximum reasonable error in the parameter. More information on this assessment is given by *Read et al.* [2007, Appendix A].

[17] In examining the results of these tests, we observe that the various perturbations all cause a multiplicative change, but also cause extra random differences. The random differences are generally smaller than the retrieved precision and we assume that they go to make up some of the observed scatter in the data shown in Figure 5. In the remainder of this section we assess the purely systematic effects of the perturbations. We quantify these effects by assuming that mixing ratio in a perturbed test, x_p, is a multiple of that in the base case, x_b, so that $x_p = kx_b$. We estimate k by performing a least-squares fit with k as the only adjustable parameter and present the results as a percentage error ($|100 * (k - 1)|$).

2.5.1. Gain Compression

[18] This error originates from the spectral signature introduced in calibrated MLS radiances by departures from a linear response within the signal chains; it can lead to errors of ±5–10% at most altitudes, with worst case errors of 25% at some levels in the lower stratosphere.

2.5.2. Standing Waves

[19] This error reflects the contribution of standing waves within the MLS instrument to the calibrated radiances. The error can be up to ±10% below 35 km, dropping to a small percentage above that.

2.5.3. Scan Jitter

[20] This is essentially a random error in pointing which occurs because the motion of the scan actuator is not perfectly smooth. Its effect as judged by this test is very small: ±1% in the lower stratosphere falling to less than ±0.5% at higher altitudes.

2.5.4. Field-of-View Shape Uncertainty

[21] For these tests the antenna shape was expanded by a factor equivalent to the 2-σ error in the beam width. it This has little effect for the 240 GHz radiometer but causes errors in CO in the lower stratosphere of 4–8% for the 118 GHz radiometer (which provides temperature/pointing). This is presumably because that radiometer operates at a longer wavelength and hence has a broader antenna pattern. This in turn makes it more sensitive to how well that pattern is characterized.

2.5.5. Sideband Fraction

[22] The sideband fraction is the fraction of the radiance recorded by the radiometer that comes from a particular sideband. This was measured during the prelaunch calibration of the instrument [*Jarnot et al.*, 2006].

[23] The sideband fractions of the 240 GHz radiometer contribute a ±3% error. The sideband fractions of other radiometers have essentially no effect on CO.

2.5.6. Antenna Offset

[24] The MLS antenna effectively points to a slightly different tangent height for each sideband of each band. Full details and an error estimate are given by *Cofield and Stek* [2006]. CO is affected by the offsets of two bands: its own band (B9F), and the O_2 band (B1F) at 118 GHz used for temperature and pointing. These were tested separately. The offset angle for B1F was perturbed by 0.002°, leading to differences of about 5–10% in CO mixing ratio. The offset angle for B9F was also perturbed by 0.002° in both sidebands. This lead to differences of 3–5% in the upper stratosphere/lower mesosphere and 15–25% in the middle-lower stratosphere.

2.5.7. Spectroscopy

[25] The forward model requires several spectroscopic parameters for each spectral line. Most of these parameters are known very accurately, for example, the line center frequency is known to within 0.5 kHz, and the line intensity to well within 1% [*Pickett et al.*, 1996]. Other parameters are poorly known, but large errors in them have a small effect on the retrieved product; the pressure shift is the most obvious example. The critical parameter for most lines is the pressure broadening coefficient. We have run several tests in which the pressure broadening coefficients of all lines for a given species were perturbed. The only species significant for CO are CO itself, O_3 and O_2. The CO, O_2 and O_3 line widths were perturbed by 5%, 3% and 3% respectively, these being the approximate uncertainties in the line widths. The perturbations caused maximum errors in the retrieved mixing ratio of 5%, 20% and 30%. The large percentage errors caused by the O_2 and O_3 line widths occur only in the lower stratosphere where the CO mixing ratio is very small.

2.5.8. Clouds

[26] Clouds have a very large effect on the retrieval of CO in the upper troposphere. They have no direct effect on the middle atmosphere measurements, but can have some indirect effects on the retrieved mixing ratio as the tropospheric and middle-atmospheric values are retrieved together. Testing suggests that this effect is small, adding ±5% extra random error and less than ±1% nonrandom error. However, the presence of clouds in the troposphere is one reason for convergence failure. Proper use of the ''Convergence'' values as described in section 2.3 should ensure that profiles affected in this way are not used for scientific studies.

2.5.9. A Priori

[27] We tested the effect of a different a priori on the retrieval. The perturbed a priori was generated as follows: (1) For $P < 100$ hPa, multiply current a priori by 2.0. (2) For $P \geq 100$ hPa, The larger of current a priori $\times 2.0$ and current a priori +50 ppbv.

[28] The results suggest that a poor a priori could introduce errors of around ±5–15%. Separate tests demonstrated that using a different a priori for temperature, water vapor or ozone causes less than 1% bias and adds only 5% extra randomness to the CO retrieval.

2.5.10. Summary of Systematic Errors

[29] The various sources of systematic error are summarized in Figure 6. At most altitudes, the main error sources are retrieval numerics, followed by gain compression. In the mesosphere, spectroscopic and antenna offsets provide the next largest contributions, while standing waves are the next most important error in the stratosphere. In the lower stratosphere, spectroscopy of the O_2 lines becomes even more important than gain compression. An a priori profile which is too dissimilar to the true profile has the potential to be as significant as gain compression in the mesosphere and the dominant systematic error source in the lower stratosphere. It is somewhat unsatisfactory that numerical issues in the retrieval are such a large contributor to the systematic

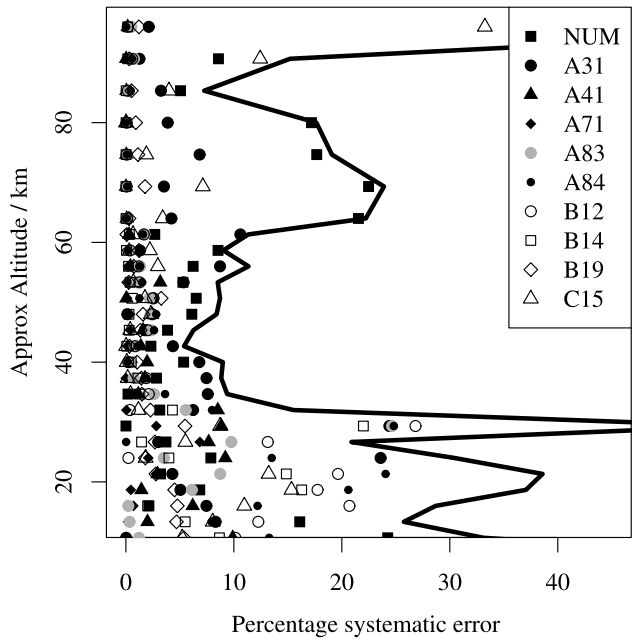

Figure 6. Systematic percentage error caused by each of the significant error sources described in the text. The three-digit codes indicate different systematic error tests as follows: NUM, retrieval numerical issues; A31, gain compression; A41, standing waves; A71, 118 GHz field-of-view shape; A83, radiometer 1 offset; A84, radiometer 3 offset; B12, O_2 spectroscopy; B14, O_3 spectroscopy; B19, CO spectroscopy; C15, CO a priori. The thick black line is the root-sum-square combination of all the error sources shown.

error. We note that this situation is not specific to CO but is true of other MLS products as well.

2.6. Differences Between v2.2 and v1.5

[30] The first public release of the MLS data was called version 1.5. In the preparation of version 2, a number of changes were made which affect the CO product, most important of which was to correct an error in the handling of the DACS data. As a result, the mixing ratios in the mesosphere decreased by 30% bringing them more closely into line with the ACE-FTS and SMR data discussed in section 4. There were also changes to the spectroscopy and to the a priori errors used. A combination of all of these changes resulted in the suppression of large and unphysical vertical oscillations in the CO profiles, especially in the 50–60 km region. This problem was not completely eliminated from v2.2, and traces of it can be seen in Figures 5, 8 and 10 later in this paper. Since the start of version 2.2 processing, the software has been updated once in order to ensure correct handling of some very rare error conditions. At this point, the specific version number was changed from 2.20 to 2.21.

3. Internal Consistency and Basic Validation

[31] Before comparing the MLS data to colocated measurements, we first ask if the retrieval is internally consistent and if the results look qualitatively similar to models and to earlier measurements of CO. We have already confirmed, in section 2.2, that the radiance residuals are generally small, that is, that the retrieved profiles are consistent with the measured radiances.

3.1. Consistency at Colocated Measurements

[32] The MLS measurement track crosses itself many times in the course of a day. This means that there are many places at which MLS makes two measurements approximately 12 hours apart, separated by less than 90 km. We take all such pairs of profiles for a day, average the difference between the profile x_a from the ascending leg of the orbit and that from the descending leg, x_d. Figure 7 shows both the mean difference

$$\Delta x_{\text{mean}} = \overline{x_a - x_d}$$

and the root-mean-square (rms) difference

$$\Delta x_{\text{rms}} = \sqrt{\overline{(x_a - x_d)^2}}$$

[33] For atmospheric variability much less than the measurement noise, we would expect the RMS difference to be $\sqrt{2}\times$ the noise level on an individual profile. We observed in section 2.4.2 that this noise level is about $0.7\times$ the quoted precision, so we should expect the RMS difference to be very similar to the quoted precision. Figure 7 shows that this is indeed the case. The mean difference should, of course, be small in some sense. For a test with n coincident pairs, we expect it to be smaller by a factor of $\sqrt{n}$ than the RMS difference. In the example shown, $n = 196$ and $\sqrt{n} \approx 14$ so the mean differences, which are around 1/14 of the RMS differences, can be considered satisfactory.

3.2. Comparison With SOCRATES

[34] SOCRATES [*Khosravi et al.*, 2002] is the National Center for Atmospheric Research (NCAR) 2-D chemical transport model. The vertical range of the model is from the ground to 120 km with a resolution of 1 km. The latitudinal resolution is 5°. Both the code and a sample of the model's output may be obtained from http://acd.ucar.edu/models/SOCRATES. We show in Figure 8 the CO field from the SOCRATES sample output for 23 July in the ninth year of the run and the weekly zonal mean MLS data from 20–26 July 2006. The two fields show the same general features: low values in the stratosphere, a rapid increase with height in the mesosphere, strong descent in the southern polar vortex and some signs of ascent over the summer pole. The most obvious differences are in the lower stratosphere where SOCRATES does not show as small values at 25 km, or as large values in the tropopause region as MLS.

3.3. Comparison With ISAMS

[35] ISAMS was a limb-sounding infrared radiometer which flew on the UARS satellite. ISAMS made the first daily global measurements of CO in the middle atmosphere which were of sufficient quality for detailed studies [*Lopez-Valverde et al.*, 1996]. (The first satellite measurements

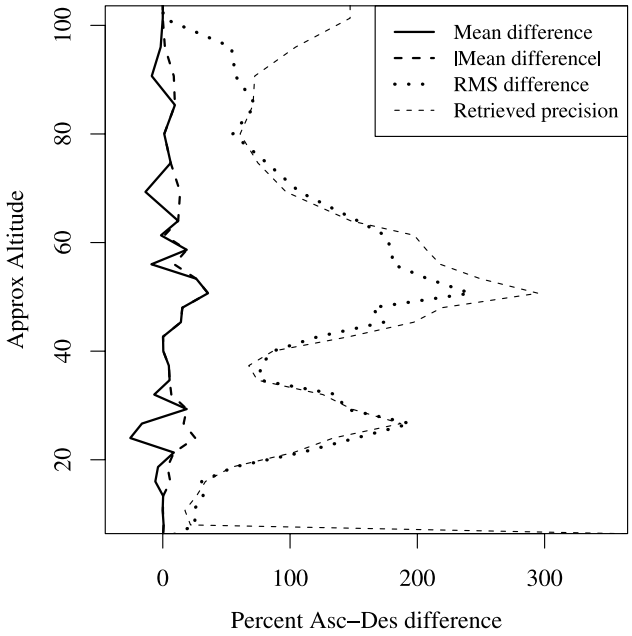

Figure 7. Percent differences between ascending and colocated descending measurements. Results are the mean of 238 pairs of profiles, each pair separated by less than 70 km. The data are from 28 January 2005. |Mean difference| means the absolute value of the mean difference.

were made by the SAMS instrument on Nimbus 7 [*Barnett et al.*, 1985]; the noise level of the SAMS measurements was such that many days data had to be averaged together to retrieve a profile.) The infrared pressure modulation technique was used for the ISAMS CO measurement. Owing to technical problems with the instrument, data are only available from 26 September 1991 to 18 January 1992 and from 27 March to 2 June and 19–22 July of 1992. We show in Figure 9 a zonal mean of ISAMS CO for the end of April 1992 and a weekly zonal mean of MLS CO for a similar period in 2007. The two data sets show the same general features: a rapid increase in CO mixing ratio with height and descent of CO-rich air into the polar vortex. Away from the vortex, the MLS CO mixing ratio increases more rapidly with height than that from ISAMS. This is probably because the vertical resolution of the ISAMS CO is 7–11 km while that of MLS is 4–7 km.

4. Comparisons With Correlative Measurements of CO

[36] We compare the MLS data to two other remotely sensed data sets: ACE-FTS and ODIN-SMR. Both instruments began operating before the launch of Aura and are still operating at the time of writing. As neither the ACE-FTS nor the SMR data are yet fully validated, agreement or disagreement with them does not necessarily confirm the quality, or lack of it, of the MLS data. Rather, the comparison between these three new data sets provides a view of our current ability to remotely sense CO mixing ratios in the middle atmosphere.

[37] We interpolate each correlative profile onto the pressure levels used by MLS giving a profile x_c. For each correlative profile we then locate x_m the MLS profile from the same day that is geographically closest. The MLS coverage means that this profile will be no further away than 12° in longitude and 0.75° in latitude. We then calculate the mean difference

$$\Delta x_{\text{mean}} = \overline{x_m - x_c}$$

and the root-mean-square (rms) difference

$$\Delta x_{\text{rms}} = \sqrt{\overline{(x_m - x_c)^2}}$$

[38] For the comparison to be entirely satisfactory, Δx_{rms} should be the same as the combined error of the two data sets, while Δx_{mean} should be much smaller. Because the CO

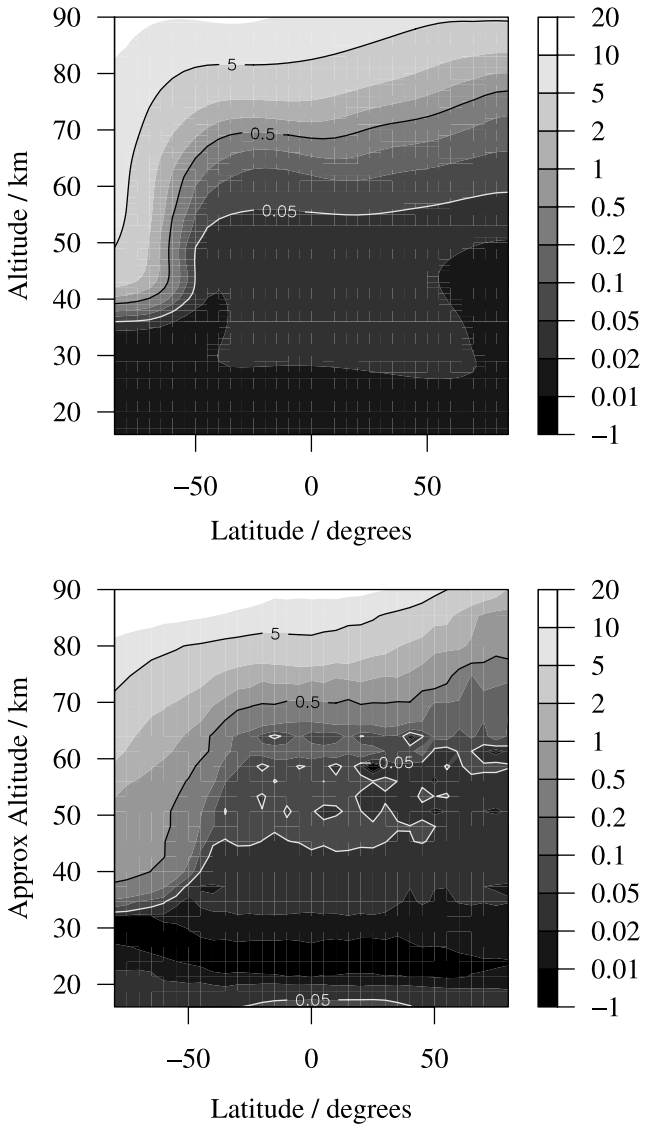

Figure 8. (top) CO field from the SOCRATES 2-D model. The data are taken from 23 July in the ninth year of the model run. (bottom) Weekly zonal mean MLS CO from 20 to 26 July 2006.

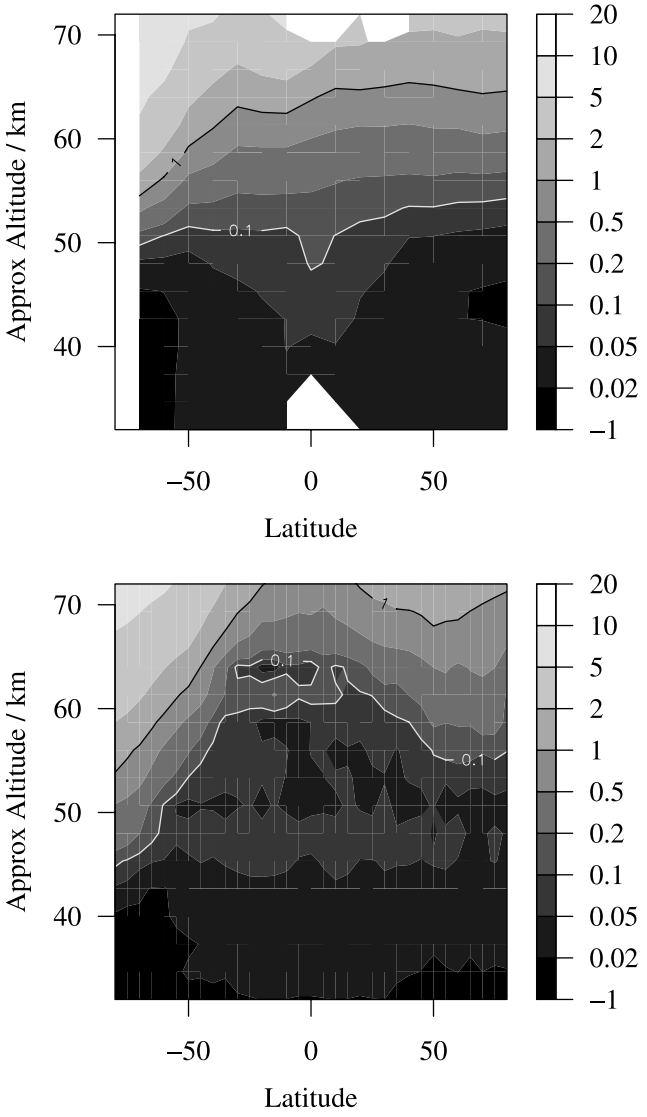

Figure 9. (top) Zonal mean ISAMS CO mixing ratio for 30 April and 4 May 1992. Two days are used, one each side of a UARS yaw, to cover a wider range of latitudes. Only daytime data are shown as ISAMS CO can be retrieved over a wider vertical range for a sunlit atmosphere. (bottom) Weekly zonal mean MLS CO mixing ratio for 28 April to 4 May 2007.

mixing ratio varies so rapidly with height, we plot these differences as percentages: 100 * $\Delta x_{\text{mean}}/\overline{x_c}$ and 100 * $\Delta x_{\text{rms}}/\overline{x_c}$.

4.1. Comparison With ACE-FTS

[39] The Atmospheric Chemistry Experiment, or ACE, (otherwise known as SCISAT-1) is a Canadian-led satellite mission launched in August 2003 into a circular orbit inclined at 74° to the equator [*Bernath et al.*, 2005]. The primary instrument is the ACE-FTS, a Fourier transform spectrometer with broad spectral coverage in the infrared (750–4400 cm^{-1}) and high spectral resolution (0.02 cm^{-1}) with a maximum optical path difference of 25 cm. Operating in solar occultation, the ACE-FTS features a high signal-to-noise ratio (SNR) but has limited geographical coverage, measuring up to 32 occultations per day. The altitude sampling of the ACE-FTS measurements varies from ≈1.5 to 6 km, but the altitude resolution is 3–4 km,

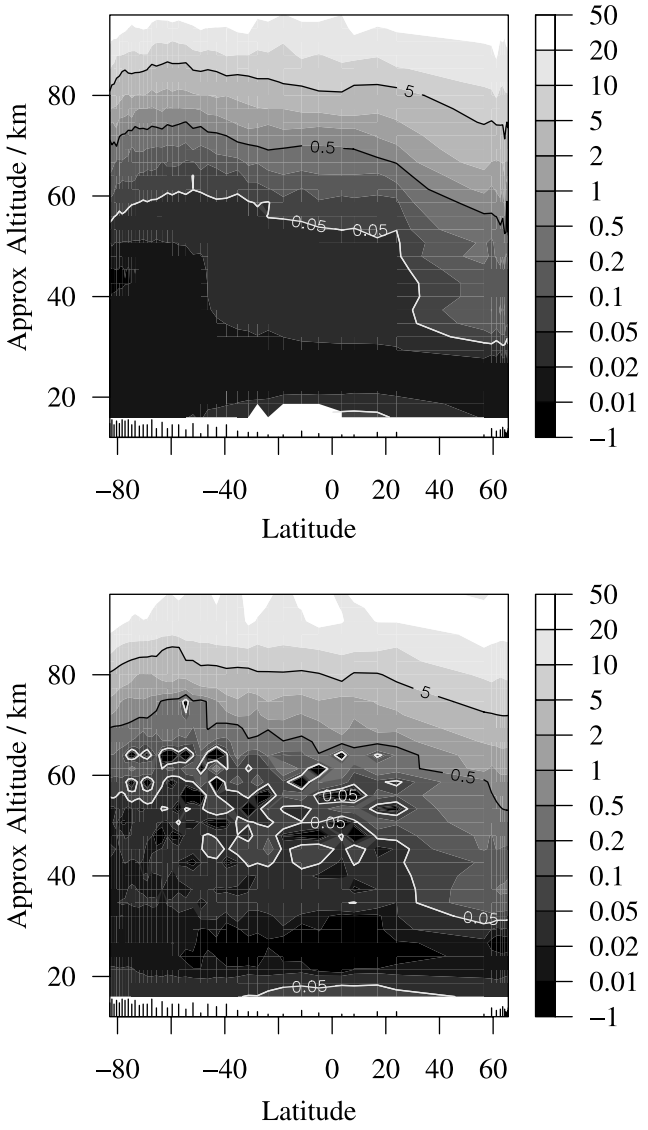

Figure 10. (top) ACE-FTS CO mixing ratios for days 31–83 of 2005. The data shown are for sunrise. The sunrise latitude moves southward during this period, so day 83 is at the left-hand side of the figure. The ticks near the bottom of the figure show the mean ACE-FTS latitude for each of the days plotted; the length of each tick is proportional to the number of ACE-FTS sunrise profiles on that day. (bottom) MLS CO mixing ratios for days 31–83 of 2005. For each ACE-FTS sunrise profile we take the five best colocated MLS profiles and average together all such profiles for the day, in order to reduce noise. The data have been smoothed in latitude, with a smoothing length of 3°: this reduces noise further where the ACE-FTS sunrise latitude changes only slightly from day to day, while having little effect in regions where the sunrise latitude changes rapidly.

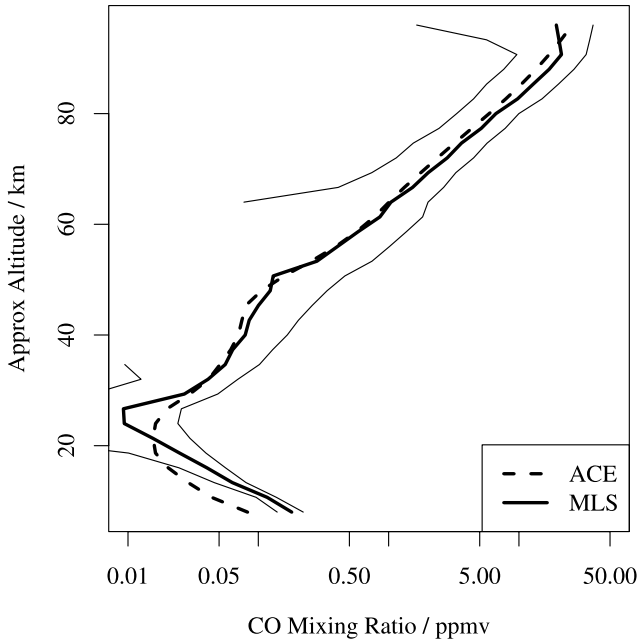

Figure 11. Means of ACE-FTS and of MLS CO profiles from all available coincident profile pairs. There were 2484 such pairs available, spread between September 2004 and October 2006. The thin lines are the mean MLS single profile retrieved precisions as provided with the data. Note that the bias between the two instruments is approximately 20–30% throughout the mesosphere. It becomes larger in percentage terms in the stratosphere as the mixing ratio is so small.

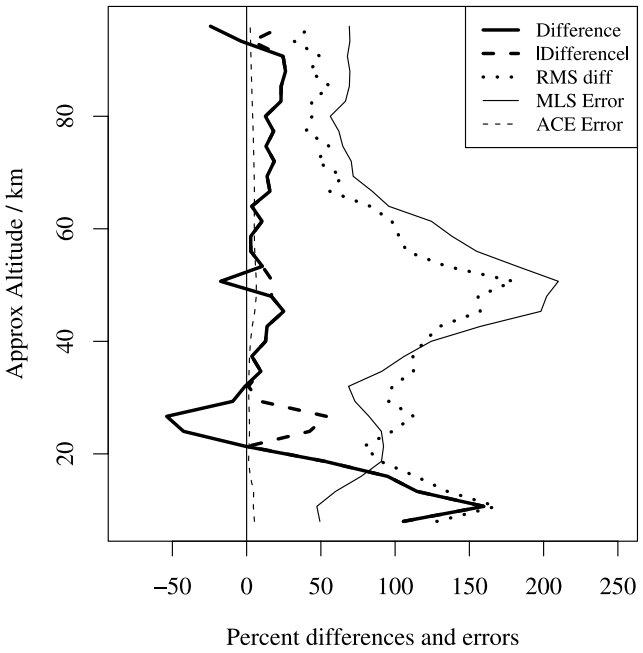

Figure 12. Differences between ACE-FTS and MLS expressed as percentages of the ACE-FTS mixing ratio. The same set of coincident profile pairs are used as in Figure 11. In both cases the errors shown are single-profile retrieved precisions; the meaning of these for MLS is described in section 2.4.2.

limited by the instrument's field of view. The procedure for ACE-FTS retrievals is described by *Boone et al.* [2005] and the CO data were first presented by *Clerbaux et al.* [2005]. The data presented here are ACE-FTS version 2.2 results. The ACE-FTS CO retrievals above 8 km employ 23 CO lines in the 1-0 band, spanning a wave number range 2086–2207 cm^{-1}. The SNR in this region is over 300:1. Results below 15 km also make use of 8 lines in the 2-0 band of CO in the range 4209–4286 cm^{-1}, where the SNR is about 30:1.

[40] We display the ACE-FTS and coincident MLS data by taking an ACE-FTS north-south sweep, and plotting the mean daily profiles (Figure 10). To reduce noise, we average the five closest MLS profiles to each ACE-FTS profile. It is clear that there are many similarities between the two data sets, although the MLS data are more noisy and ragged, particularly near 60 km. We note in particular the high mixing ratios in the northern polar vortex.

[41] The biases between the two instruments can be seen more clearly in Figure 11, which shows mean profiles, and Figure 12, which shows percentage differences. The biases are about 50% in the lower stratosphere where the mixing ratios are very small. In the mesosphere, MLS mixing ratios are consistently 25% higher than those from ACE-FTS. This is consistent with the systematic errors which we estimated in section 2.5. Additional comparisons between ACE-FTS and MLS CO are shown by *Manney et al.* [2007]; they are generally consistent with the results shown here.

4.2. Comparison With ODIN SMR

[42] The Submillimetre Radiometer (SMR) forms the bulk of the payload of the ODIN satellite [*Murtagh et al.*, 2002]. It operates on a similar principle to MLS, but has a

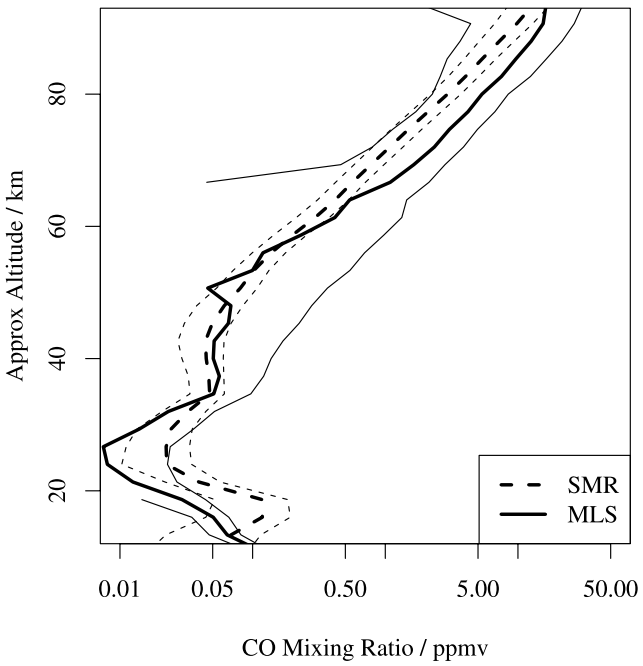

Figure 13. Mean of all SMR and all colocated MLS profiles for 13 January to 2 February 2006. The thin lines are the quoted errors for a single profile measurement.

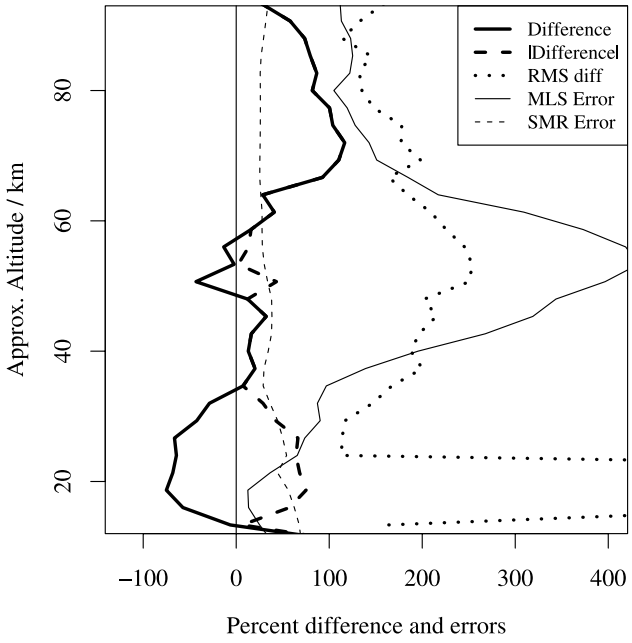

Figure 14. Differences between SMR and MLS for 13 January to 2 February 2006, expressed as percentages of the SMR mixing ratio. The errors shown are the single-profile retrieved precisions for the two instruments; the meaning of these for MLS is described in section 2.4.2.

more complex mission; in addition to limb sounding of the atmosphere it is also capable of radio astronomy measurements. Timesharing between several aeronomy modes and radioastronomy observations means that SMR makes measurements of CO for about 3 d per month on average. SMR measured CO continuously for a period in late January and early February 2006; we use this period for our comparison with MLS. The SMR CO retrieval is described by *Dupuy et al.* [2004]. The resulting data have been compared to ACE-FTS by *Jin et al.* [2005].

[43] The SMR data show qualitatively similar features to MLS, ACE-FTS, ISAMS and SOCRATES. We make a quantitative comparison between SMR and MLS by taking all colocated pairs of profiles for the period 13 January to 2 February 2006, and calculating the mean difference and the RMS difference. SMR profiles are only used if the quality flag is set to 0, 4 or 8: profiles with any other value are rejected as this indicates that the retrieval did not converge (B. Barret, personal communication, 2006). Results are shown in Figures 13 and 14. We note that in the mesosphere, MLS shows a positive bias with respect to SMR, as it did with respect to ACE-FTS. However the MLS-SMR bias is larger in the upper mesosphere, typically in the 50–100% range. In the lower stratosphere, the MLS values are much lower than the correlative measurements, as was the case in the comparison with ACE-FTS.

5. Summary and Conclusions

[44] The MLS instrument has made the most extensive set of measurements of CO in the middle atmosphere to date. We have shown that the retrieved V2.2 product is internally consistent and has the same general features as CO in models and historical measurements. Comparisons with coincident measurements suggest that the MLS mixing ratios have a high bias in the mesosphere. The comparison with ACE-FTS implies that this bias is about 25%, which is not much larger than the systematic errors discussed in section 2.5. The comparison with ODIN-SMR shows differences of up to 100% in some parts of the mesosphere. These differences are too large to be accounted for by the systematic errors assessed in section 2.5; it seems likely that they are in part due to systematic errors in the SMR data. The precision and resolution of the data are summarized in Table 2.

[45] Validation is an ongoing process. We can expect our understanding of the data to grow as more days are processed and other sources of correlative data become available. We nevertheless consider the data to be usable for a variety of scientific studies. Possible applications include the dynamics of the mesosphere, particularly the stratopause region and the photochemistry of CO itself and associated species such as CH_4 and OH. The descent of CO into the polar vortex makes it a useful tracer for studies of the upper stratosphere in the polar winter.

Table 2. Summary of Single-Profile Precision, Resolution, and Systematic Biases for MLS Version 2.2 CO[a]

Pressure, hPa	Resolution, km, Vertical × Horizontal	Precision, ppmv	Systematic Error, %	Systematic Differences	Comment
<0.001	—	—	—	—	not retrieved
0.001	—	—	—	—	unsuitable for scientific study
0.0022	9 × 200	11	±20%	+25	
0.01	7 × 200	3.0	±20%	+20%	
0.046	6.5 × 200	1.1	±20%	+20%	
0.14	3 × 200	0.9	±10%	+15%	
1	3 × 230	0.2	±10%	+10%	
10	3 × 300	0.028	±30%	+10%	
31	3 × 300	0.016	±30%	−60%	
100	4 × 330	0.016	±30%	+50%	
>100	—	—	—	—	see *Livesey et al.* [2007]

[a]The horizontal resolution is along the measurement track. Across the track, the footprint is 6 km wide but the tracks are 24° of longitude apart. Precisions are the retrieved precision as provided with the data and may be interpolated between the pressures in the table. Systematic bias is calculated from the tests described in section 2.5. Systematic differences are taken from the comparison against ACE-FTS data.

[46] **Acknowledgments.** The authors thank the SOCRATES team for making the model and its output available. MLS research in the UK is funded by NERC. The ACE mission is supported primarily by the Canadian Space Agency. Work at the Jet Propulsion Laboratory, California Institute of Technology, was carried out under a contract with NASA. The authors also thank L. J. Kovalenko for helpful comments on the text and R. E. Cofield, V. Perun and P. A. Wagner for helpful information about the galactic core.

References

Allen, D. R., J. L. Stanford, M. A. López-Valverde, N. Nakamura, D. J. Lary, A. R. Douglass, M. C. Cerniglia, J. J. Remedios, and F. W. Taylor (1999), Observations of middle atmosphere CO from the UARS ISAMS during the early northern winter 1991/1992, *J. Atmos. Sci.*, *56*, 563–583.

Barnett, J. J., M. Corney, A. K. Murphy, R. L. Jones, C. D. Rodgers, F. W. Taylor, W. J. Williamson, and N. M. Vyas (1985), Global and seasonal variability of the temperature and composition of the middle atmosphere, *Nature*, *313*, 439–443.

Bernath, P. F., et al. (2005), Atmospheric chemistry experiment (ACE): Mission overview, *Geophys. Res. Lett.*, *32*, L15S01, doi:10.1029/2005GL022386.

Boone, C. D., R. Nassar, K. A. Walker, Y. Rochon, S. D. McLeod, C. P. Rinsland, and P. F. Bernath (2005), Retrievals for the atmospheric chemistry experiment Fourier-transform spectrometer, *Appl. Opt.*, *44*(33), 7218–7231.

Chipperfield, M. P. (1999), Multiannual simulations with a three-dimensional chemical transport model, *J. Geophys. Res.*, *104*, 1781–1805.

Clerbaux, C., et al. (2005), Carbon monoxide distribution from the ACE-FTS solar occultation measurements, *Geophys. Res. Lett.*, *32*, L16S01, doi:10.1029/2005GL022394.

Cofield, R. E., and P. C. Stek (2006), Design and field-of-view calibration of 114–640 GHZ optics of the Earth Observing System Microwave Limb Sounder, *IEEE Trans. Geosci. Remote Sens.*, *44*(5), 1166–1181.

Combes, F. (1991), Distribution of CO in the Milky Way, *Annu. Rev. Astron. Astrophys.*, *29*, 195–237.

Dupuy, E., et al. (2004), Strato-mesospheric measurements of carbon monoxide with the Odin sub-millimetre radiometer: Retrieval and first results, *Geophys. Res. Lett.*, *31*, L20101, doi:10.1029/2004GL020558.

Jarnot, R. F., V. S. Perun, and M. J. Schwartz (2006), Radiometric and spectral performance and calibration of the GHz bands of EOS MLS, *IEEE Trans. Geosci. Remote Sens.*, *44*(5), 1131–1143.

Jin, J. J., et al. (2005), Co-located ACE-FTS and Odin/SMR stratospheric-mesospheric CO 2004 measurements and comparison with a GCM, *Geophys. Res. Lett.*, *32*, L15S03, doi:10.1029/2005GL022433.

Khosravi, R., G. Brasseur, A. Smith, D. Rusch, S. Walters, S. Chabrillat, and G. Kockarts (2002), Response of the mesosphere to human-induced perturbations and solar variability calculated by a 2-D model, *J. Geophys. Res.*, *107*(D18), 4358, doi:10.1029/2001JD001235.

Livesey, N. J., W. V. Snyder, W. G. Read, and P. A. Wagner (2006), Retrieval algorithms for the EOS Microwave Limb Sounder (MLS) instrument, *IEEE Trans. Geosci. Remote Sens.*, *44*(5), 1144–1155.

Livesey, N. J., et al. (2007), Validation of Aura microwave limb sounder O_3 and CO observations in the upper troposphere and lower stratosphere, *J. Geophys. Res.*, doi:10.1029/2007JD008805, in press.

Lopez-Valverde, M. A., M. Lopez-Puertas, J. J. Remedios, C. D. Rodgers, F. W. Taylor, E. C. Zipf, and P. W. Erdman (1996), Validation of measurements of carbon monoxide from the improved stratospheric and mesospheric sounder, *J. Geophys. Res.*, *101*(D6), 9929–9955.

Manney, G. L., et al. (2007), Solar occultation satellite data and derived meteorological products: Sampling issues and comparisons with Aura MLS, *J. Geophys. Res.*, doi:10.1029/2007JD008709, in press.

Murtagh, D., et al. (2002), An overview of the Odin atmospheric mission, *Can. J. Phys.*, *80*(4), 309–319.

Oka, T., T. Hasegawa, T. Handa, M. Hayashi, and S. Sakamoto (1996), CO ($J = 2 - 1$) line observations of the galactic center molecular cloud complex. I. On-plane structure, *Astrophys. J.*, *460*, 334–342.

Pickett, H. M., R. L. Poynter, E. A. Cohen, M. L. Delitsky, J. C. Pearson, and H. S. P. Müller (1996), Submillimeter, millimeter and microwave spectral line catalog, NASA Jet Propul. Lab., Pasadena, Calif. (Available at http://spec.jpl.nasa.gov/)

Read, W. G., et al. (2007), Aura microwave limb sounder upper tropospheric and lower stratospheric H_2O and RHi validation, *J. Geophys. Res.*, doi:10.1029/2007JD008752, in press.

Rodgers, C. D. (2000), *Inverse Methods for Atmospheric Sounding: Theory and Practise*, World Sci., Hackensack, N. J.

Schoeberl, M. R., et al. (2006), Overview of the EOS Aura mission, *IEEE Trans. Geosci. Remote Sens.*, *44*(5), 1066–1074.

Solomon, S., R. R. Garcia, J. J. Olivero, R. M. Bevilacqua, P. R. Schwartz, R. T. Clancy, and D. O. Muhleman (1985), Photochemistry and transport of carbon monoxide in the middle atmosphere, *J. Atmos. Sci.*, *42*, 1072–1083.

Waters, J. W. (2006), The Earth Observing System Microwave Limb Sounder (EOS MLS) on the Aura satellite, *IEEE Trans. Geosci. Remote Sens.*, *44*(5), 1106–1121.

Waters, J. W., W. J. Wilson, and F. I. Shimabukuro (1976), Microwave measurement of mesospheric carbon dioxide, *Science*, *191*, 1171–1172.

B. Barret and P. Ricaud, Laboratoire d'Aerologie, UMR 5560 CNRS/Université Paul Sabatier, Observatoire de Midi-Pyrenees, 14 Avenue Edouard Belin, F-31400 Toulouse, France. (barp@aero.obs-mip.fr; philippe.ricaud@aero.obs-mip.fr)

P. Bernath, Department of Chemistry, University of York, York YO10 5DD, UK. (pfb500@york.ac.uk)

C. Boone, Department of Chemistry, University of Waterloo, 200 University Avenue W, Waterloo, ON, Canada N2L 3G1. (cboone@acebox.uwaterloo.ca)

C. Clerbaux, Service d'Aéronomie, Boîte 102, Université Pierre et Marie Curie, 4 Place Jussieu, F-75252 Paris Cédex 05, France. (ccl@aero.jussieu.fr)

M. J. Filipiak and H. C. Pumphrey, School of Geosciences, University of Edinburgh, Edinburgh EH9 3JN, UK. (mjf@staffmail.ed.ac.uk; h.c.pumphrey@ed.ac.uk)

R. F. Jarnot, N. J. Livesey, G. L. Manney, M. J. Schwartz, and J. W. Waters, Jet Propulsion Laboratory, 4800 Oak Grove Drive, Mail Stop 183-701, Pasadena, CA 91109-8099, USA. (jarnot@mls.jpl.nasa.gov; nathaniel@mls.jpl.nasa.gov; manney@mls.jpl.nasa.gov; michael@mls.jpl.nasa.gov; joe@mls.jpl.nasa.gov)

K. A. Walker, Department of Physics, University of Toronto, 60 St. George Street, Toronto, ON, Canada M5S 1A7. (kwalker@atmosp.physics.utoronto.ca)